Available online at www.sciencedirect.com
SCIENCE DIRECT®
Journal of Sound and Vibration 281 (2005) 815–834
JOURNAL OF SOUND AND VIBRATION
www.elsevier.com/locate/jsvi

Non-synchronous rotating damping effects in gyroscopic rotating systems

Eugenio Brusa*, Giacomo Zolfini

Department of Electrical, Managerial and Mechanical Engineering, Universitá degli Studi di Udine, Via delle Scienze 208, I-33100, Udine, Italy

Received 18 October 2003; accepted 2 February 2004
Available online 15 September 2004

Abstract

The effects of non-synchronous rotating damping, i.e., of energy dissipation in elements rotating at a speed different from that of the main rotor, on the dynamic behaviour of the latter have been already studied in a previous paper (J. Rotating Machinery 6 (6) (2000)) for the case of non-gyroscopic rotating systems. A planar model, namely the Jeffcott's rotor, was used. The present study is aimed at investigating, through analytical and numerical models, the behaviour of rotors having a non-negligible gyroscopic effect. The parameters of the system affecting the dynamic stability are identified and the threshold of instability is then computed. A sort of map of stability is provided to allow mechanical engineers predicting possibile range of instability for forward and backward whirling motions. An experimental validation on a simple test rig is presented in order to show the effectiveness of the proposed stability analysis. Non-synchronous rotating damping is implemented by using a non-synchronous electromagnetic damper based on eddy currents.

1. Motivation

The literature on rotordynamics [1–3] usually includes detailed analysis of the role of non-rotating and synchronously rotating damping on the dynamic stability of rotors. It is well known

*Corresponding author. Tel.: +39-0432-558299; fax: +39-0432-558251.
E-mail address: eugenio.brusa@uniud.it (E. Brusa).

0022-460X/$ - see front matter © 2004 Elsevier Ltd. All rights reserved.
doi:10.1016/j.jsv.2004.02.019

that they play a different role in the dynamic stability of the rotating system in subcritical and supercritical regimes of the spin speed: non-rotating damping is always stabilizing in both fields, rotating damping has a destabilizing effect on forward whirling motions in supercritical regime, while backward whirls are naturally stable. This knowledge in the past was suitable for interpreting several failures that occurred in industrial and space systems, due to the dynamic instability [4].

More recently new applications deal with multibody rotors, in which several rotating bodies are either connected to each other by elastic joints (like in space mechanisms and spacecrafts) [5,6] or constrained to the same stator [2]. The so-called dual rotors [2] are a class of rotating systems where the structural damping associated to shafts rotating in the opposite direction can be effective for the stability of vibration. Large paper printers, gearboxes, textile machines often have multiple rotating rods constrained to the same frame, rotating at different speeds and sometimes in opposite directions. Free rotors [7,8] like spinning spacecraft systems, satellites or momentum and reaction wheels are typical cases where damping associated to the different parts of the system behaves as non-synchronous. Spinning spacecraft, in which the only conventional way of applying non-rotating damping is to introduce de-spun devices, can be stabilized by introducing counter-rotating damping, through active devices like magnetic or electrostatic bearings [5,6].

In the presence of multiple rotors, problems related to the dynamic stability may occur, depending on the damping, when it is appreciated as non-synchronously rotating with respect to the spin speed of the main rotor. A non-synchronous rotating contribution corresponds to an energy dissipation occurring in parts rotating at a spin speed which is lower or higher than the angular velocity of the main rotor. A known case in the literature is already cited: lubricated bearings, where the oil film is assumed to rotate at half the spin speed [9–11]. In some situations this causes unstable behaviour, usually referred to as oil whip. The threshold of this kind of instability is in many cases approximately close to twice the first critical speed. Further examples of non-synchronously rotating damping are structural damping in shafts, rotating at different spin speeds, induction effects due to electromechanical coupling in motors, active and passive magnetic bearings and dampers, if the dissipation occurs in conductive parts rotating at various speeds.

In a previous paper [12] it was already found that two relevant conditions have to be discussed: when the non-synchronous damping is rotating in the same direction of the rotor, which can be referred to as co-rotating and when it rotates in the opposite direction, referred to as counter-rotating. In Ref. [12] a preliminary analysis was based on the Jeffcott's rotor model, i.e., plane 2 real dof's model. This model allowed realizing that co-rotating damping decreases the stability of forward whirling modes of the rotor when the rotational speed of the damper increases. This effect is due to an imaginary and negative contribution to the stiffness of the system (circulatory effect) appearing in the equation of motion of the rotor [12]. It consists of the product between the non-synchronous damping coefficient and the spin speed at which this action is exerted. The minus sign in the above term corresponds to a co-rotation of the non-synchronous effect, while an equivalent positive stiffness contribution is found when a counter-rotation occurs. A counter-rotating damping, with either low damping coefficient or acting at a lower spin speed, increases the stability of forward modes but simultaneously tends to decrease that of backward whirling modes. In the case of the Jeffcott rotor, a suitable value of the product of the non-synchronous damping coefficient and the speed, assuring the simultaneously stability of both forward and backward modes, can be found. Backward modes can become unstable if a higher value of

counter-rotating damping is achieved, while forward ones show no threshold of instability. This behaviour is quite new, since backward modes are usually assumed to be naturally stable: this was the most original result achieved by the previous analysis. The latter was performed under the assumption that no gyroscopic effect was present. Practical applications usually exhibit gyroscopic effects.

Several applications among those already mentioned include an unavoidable gyroscopic effect. This paper analyzes the joint effect between gyroscopy and non-synchronous rotating damping in terms of dynamic stability. The main tool provided to mechanical engineers shall be a stability map, taking into account the role of the non-synchronous rotating damping. To make expedient the demonstration of the effect herewith analyzed, a preliminary experimental validation has been carried out on a simple test rig. A non-synchronous damping action is induced by eddy current dampers on a conductive disc rotor, equipped with permanent magnets, either co-rotating or counter-rotating. The latter allowed showing the phenomenon itself and the dependence of the non-synchronous rotating damping on the rotational speed of the rotor. In principle, non-synchronous damping can be also synthesized in active devices, without resorting to a damper rotating at the required speed, by supplying a suitable control law to the magnetic force in a such a way that it appears to be co-rotating or counter-rotating. This application is particularly interesting for statorless rotors, e.g., spinning spacecrafts, where stability can be achieved even in cases for which passive stabilization is difficult [6,13].

2. System modelling

2.1. A didactic demonstrator for preliminary experiments

To make expedient the discussion of the topic herewith investigated a simple didactic demonstrator was built to visualize the relevant dynamic effects of non-synchronous damping on a disc rotor. A preliminary description is proposed here to deal quite easily with the analytical formulation of the model, including the equations of motion of the whole system.

The demonstrator was conceived to be as much as possible a typical four real dof rotor, easily analyzed by the well-known model proposed in the literature [3]. It consists (see Figs. 1 and 2 including, respectively, a pitcure and a sketch of the system) of two rotating systems: a rigid frame, composed of two horizontal and one vertical thick plates in aluminium, holds at the top of a first pendulum rotor, a disc being suspended by a quill steel shaft, and at the bottom a second disc rotor, both fed by brushless motors. Around this axisymmetric system of two rotors a sort of rotating platform has been built, composed of two circular plates and a plexiglass cylindric body. This body is connected to the first pendulum rotor and rotates at the same angular velocity. This way it resembles a satellite platform with an internal suspended mass, with non-negligible gyroscopic effects. Originally, it was required to make the demonstrator suitable for a critical review of the rotordynamic behaviour of the satellite Galileo Galilei [6]. To detect the lateral displacements along two perpendicular radial directions of the isotropic pendulum rotor a couple of optical sensors was mounted on the base of the rotating platform, as it should be done in a spacecraft system (actually both figures show only one sensor to make it easier to understand the layout of the test rig).

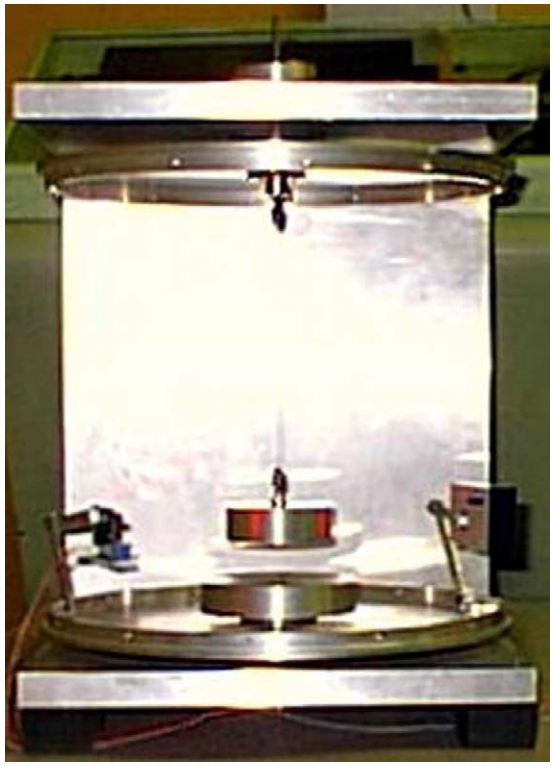

Fig. 1. Picture of the demonstrator built for the study of non-synchronous damping.

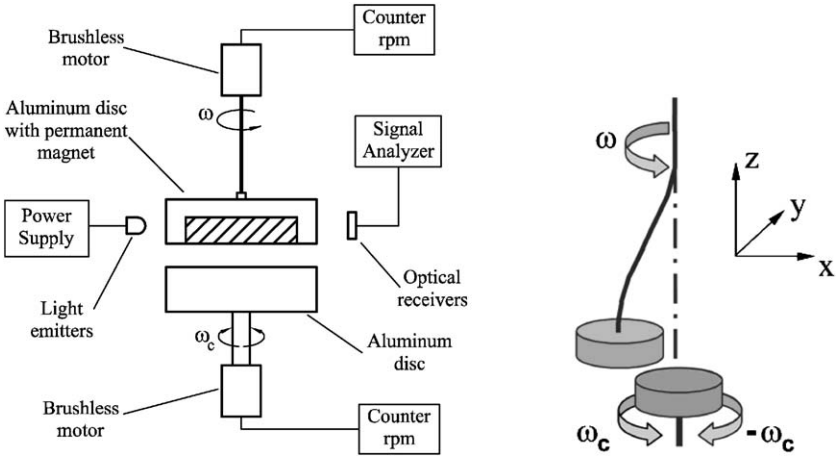

Fig. 2. Description of the experimental test rig.

If one analyzes the damping distribution in the above test rig the following can be appreciated: a non-rotating contribution applied by the structural damping and friction effects occurring in non-rotating parts of the stator (silent blocks at the bottom of the lower plate, threaded joints,

inner damping of plates), a rotating contribution due to the structural damping and friction associated to the first pendulum rotor (clamps, quill shaft, disc) and the damping effect of second rotor which can be considered either rotating or non-rotating depending on its temporary dynamic status. No coupling is present between the first and the second rotor without an explicit coupling action, which was provided in this case by equipping the disc of the top rotor with a permanent magnet being able to induce eddy currents in the conductive material of the second disc. If the disc with the magnet is placed at a small distance from the aluminium disc, the latter works as an eddy current damper [14,15]. Since the pendulum disc whirls, the magnetic flux lines of the supported magnet cross the bottom disc, which can be fixed (non-rotating), rotating (synchronously or not) either in the same direction (co-rotation) or in the opposite one (counter-rotating or contra-rotating). In this way the electromechanical coupling introduces the required damping effect [15]. The energy dissipation due to the eddy currents occurs in the aluminium disc supplying a damping action which is non-rotating, if the disc is fixed, co-rotating if it rotates in the same direction with respect to the disc with the magnet and counter-rotating if it spins in the opposite direction.

Although the nature of the phenomenon studied here cannot be easily investigated through experiments, because of the complexity of a system equipped with non-synchronous actions, a preliminary validation of the model has been performed on the above demonstrator. Experiments have been done to find the frequencies and the equilibrium configuration of the system in rotation, corresponding to the rotating velocities of the main rotor, consisting of the disc equipped with a permanent magnet, and the secondary rotor, consisting of the aluminium disc either co-rotating or counter-rotating. A detailed stability analysis of the whirling motions has been carried out to validate the map of stability found by modelling the system.

2.2. Construction details of the test rig

To allow a fast modelling of the above demonstrator in the following section, the relevant design parameters and the equipments details are herewith collected. Referring to the sketch in Fig. 2: the main rotor is an aluminium disc suspended by a quill steel shaft, equipped with axially polarized ferrite permanent ring magnet. The outer diameter of the disc is 68 mm and the height 22 mm, while the mass is 222 g. The shaft has a diameter of 0.5 mm and a length of 147 mm. A second disc rotor is located in the lower part of the device: it is an aluminium disc supported by a steel shaft, either co-rotating or counter-rotating with respect to the first disc. The two rotors are fed by brushless motors Oriental Motors, model HBL 540 KA, for the disc with the permanent magnet and model HBL 425 KA for the second one. Two optical sensors are mounted on the stationary part of the device. They are based on infrared diode Siemens SFH485 and on photodiode Siemens BPW34. These sensors measure the lateral displacements of the magnetic disc suspended by the thin shaft in two orthogonal directions. The displacements are recorded by a Bakker Electronics-2580 Multi Channel Waveform Analyzer. The drivers of the motor's provide a speed output signal from which it is possible to know the angular velocity of the discs through an Hameg HM8122 frequencymeter. The motor's speed is controlled by means of a simple speed potentiometer.

2.3. Rotor with 4 real dof and non-synchronous rotating damping

2.3.1. Model description

To perform a preliminary analysis of the relevant phoenomena affecting the dynamic behaviour of a gyroscopic rotating system a typical model proposed in the literature [3] is an axisymmetric shaft supporting a disc, with non-negligible mass m and moments of inertia J_t and J_p, simply supported by bearings (Fig. 3). The shaft is assumed to be ideally rigid and bearings elastic, although no lack of generality occurs if one assumes it to be a flexible shaft on rigid bearings: just in case of structural damping associated to the shaft it becomes significant where the compliance is actually located, either on statoric or rotoric part of the system. Four degrees of freedom of the centre of mass of the rotor are usually introduced into the equations of motion, namely lateral displacements x and y and rotations ϕ_y and ϕ_x about the transversal axes x and y, respectively. Nevertheless, complex notation allows reducing the dimensions of the resulting equations of motion of system [3]:

$$z = x + \mathrm{i}\, y, \tag{1}$$

$$\phi = \phi_y - \mathrm{i}\, \phi_x, \tag{2}$$

z being the complex lateral displacement and ϕ the complex rotation. The position of the disc on the shaft, described by quote a, may be relevant in terms of Campbell diagram of the whole rotor and of the critical speeds computation as in Ref. [3]. In the case of the demonstrator the shaft is clamped at one end and free on the other, where the disc is suspended. In the present investigation the above model was required to deal with the gyroscopic effect, instead of the Jeffcott's rotor, already used for the previous one, based only on the role of the co-rotating and counter-rotating damping in a non-gyroscopic system [12].

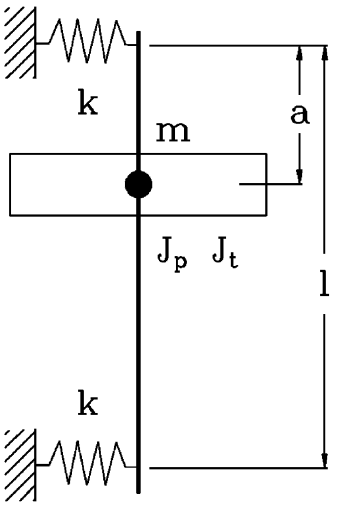

Fig. 3. Sketch of the real 4 dof's model for rotordynamics with gyroscopic effects.

2.3.2. Equations of motion

The model of a 4 real dof's rotor is suitable to analyze the combined effects of gyroscopy and the non-synchronous rotating damping, and particularly to predict the experimental behaviour of the whole demonstrator. The test case focused the dynamic behaviour of the main rotor (pendulum), while the second one is considered only as an external damper to apply non-synchronous actions. The layout of the rotor includes a disc, supported by a very flexible shaft with vertical axis, clamped at the top. A lumped parameters model can be easily obtained to reduce the whole continous system in a 4 dof's rotor. Due to the simplicity of the system a straight assumption can be made: the elastic behaviour is completely attributed to the quill shaft, i.e., the stiffness will be computed by evaluating that of the shaft, including the stiffnening effect of the pendulum, while relevant inertial properties are attributed only to the disc, and neglected for the shaft [3]. The generalized co-ordinates are the translation of the centre of gravity of the disc in x and y directions and the two rotations of the disc about x and y axes, because of the axial symmetry the complex notation [1,3] is preferred and the generalized co-ordinates vector holds

$$\{\mathbf{q}\} = \begin{Bmatrix} z \\ \phi \end{Bmatrix} = \begin{Bmatrix} x + \mathrm{i}\, y \\ \phi_y - \mathrm{i}\, \phi_x \end{Bmatrix}. \tag{3}$$

Assuming that the angular velocity of the disc and of the non-synchronous damper are constant, the linearized equation of motion of the system is

$$\mathbf{M}\,\ddot{\mathbf{q}} + (\mathbf{C} - \mathrm{i}\,\omega\,\mathbf{G})\,\dot{\mathbf{q}} + (\mathbf{K} - \mathrm{i}\,\omega\,\mathbf{C}_r - \mathrm{i}\,\omega_c\,\mathbf{C}_c)\,\mathbf{q} = \mathbf{f}, \tag{4}$$

where **M**, **G**, **C** and **K** are the inertia, gyroscopy, damping (global) and stiffness matrices; **f** is the vector of external forces and **q** is the vector of complex co-ordinates defined in Eq. (3):

$$\mathbf{q} = \begin{Bmatrix} z & \phi \end{Bmatrix}^{\mathrm{T}} \tag{5}$$

$$\mathbf{M} = \begin{bmatrix} m & 0 \\ 0 & J_t \end{bmatrix}, \quad \mathbf{G} = \begin{bmatrix} 0 & 0 \\ 0 & J_p \end{bmatrix}, \quad \mathbf{K} = \begin{bmatrix} k_{1,1} & k_{1,2} \\ k_{2,1} & k_{2,2} \end{bmatrix}, \tag{6}$$

$$\mathbf{C} = \mathbf{C}_n + \mathbf{C}_r + \mathbf{C}_c = \begin{bmatrix} c_z & c_{z\phi} \\ c_{\phi z} & c_{\phi} \end{bmatrix}, \tag{7}$$

$$\mathbf{C}_n = \begin{bmatrix} c_{z_n} & c_{z\phi_n} \\ c_{\phi z_n} & c_{\phi_n} \end{bmatrix}, \quad \mathbf{C}_r = \begin{bmatrix} c_{z_r} & c_{z\phi_r} \\ c_{\phi z_r} & c_{\phi_r} \end{bmatrix}, \quad \mathbf{C}_c = \begin{bmatrix} c_{z_c} & c_{z\phi_c} \\ c_{\phi z_c} & c_{\phi_c} \end{bmatrix}. \tag{8}$$

The subscript r stands for rotating, n for non-rotating, while the subscripts z and ϕ stand for quantities related, respectively, to translational (z) and rotational (ϕ) co-ordinates. Scalar quantities are: ω, the angular velocity of the rotor, ω_c the velocity of the non-synchronous damper, m, J_t and J_p respectively the mass, the transversal and polar moments of inertia of the disc. Vector **f** includes the generalized external forces applied to the system, including inbalances. The above equation includes several peculiarities due to the new effect investigated, which are

herewith pointed out. Under the above assumptions the inertial properties of the rotor are those of the disc and the mass and the gyroscopy matrices are consequently computed. Stiffness is only related to the quill shaft. The elements of matrix **K** can be obtained through the FEM technique by using a beam element to describe the mechanical behaviour of the shaft: beam flexural stiffness formulation can be easily used, including the constraints due to the clamp; then the stiffening effect due to the pendulum effect is applied by summing the stiffness contribution to the previous one [3]. According to the Eulero–Bernoulli beam formulation, with the shaft clamped at the upper end and connected to the centre of gravity of the disc at the other, matrix **K** is

$$\mathbf{K} = \frac{EI}{l^3}\begin{bmatrix} 12 & -6l \\ -6l & 4l^2 \end{bmatrix} + \frac{mg}{30l}\begin{bmatrix} 36 & -3l \\ -3l & 4l^2 \end{bmatrix}, \tag{9}$$

where E, l and I are the Young's elastic modulus, the length and the inertia moment of the shaft while m is the mass of the disc and g the gravitational acceleration.

Like in the case of the classic formulation of rotors with non-rotating and rotating synchrounous damping, coefficients appear twice in equation of motion: once in the term which multiplies the generalized speed vector and a second one in the term which is proportional to the generalized displacement vector. In the first one a global effect of damping appears as sum of the damping coefficients: $c_z = c_{z_n} + c_{z_r} + c_{z_c}$, $c_\phi = c_{\phi_n} + c_{\phi_r} + c_{\phi_c}$. In the second one, it is unusual that the term related to non-synchronous damping can be either positive or negative, depending on the sign of the angular speed ω_c. This means that the dangerous effect on the stability of the rotor owing to the synchronous rotating damping in supercritical regime can be attenuated directly at this level by tuning a suitable contribution of non-synchronous damping. The formulation of damping matrices $\mathbf{C}_n, \mathbf{C}_r, \mathbf{C}_c$ is based on the assumption that equivalent viscous damping coefficients can be obtained and that proportional damping can be applied [3]. In the case of the demonstrator non-rotating damping is mainly provided by the silent blocks supporting the stator under the lower plate and by the frame itself; rotating damping is mainly due to the loss factor η of the material of the shaft, while non-synchrounous contribution is due to the electromechanical coupling, i.e., eddy currents dissipation occurring in the secondary disc. Rotating damping coefficients were computed by means of an equivalent viscous damping formulation $c_{\mathrm{eq}} = \eta k/\lambda$, by approximating the frequency of the hysteresis loop λ to the frequency of the whirling motion [3]. An equivalent viscous damping formulation can be followed for the non-synchronous eddy current damper, according to and under the assumptions described in Refs. [14–16].

Numerical investigations were performed by assuming a simplified structure of the damping matrices in application to the demonstrator. While the rotating synchronous contribution can be computed through the structural damping model, holding a complete symmetric matrix in complex co-ordinates, non-rotating and non-synchronous contributions have been only characterized by diagonal matrices assuming that the cross-coupling elements of the above matrices were null or at least negligible. A second discussion was open on the role of the rotational effect of damping (elements c_{ϕ_i}) on the dynamic behaviour of the test rig, as it will appear in the section dealing with the analysis and the experimental validation. Non-synchronous damping in the test rig only provides a translational effect because of the phenomenon of current induction, mainly being based on the mutual displacement of the two discs in the presence of whirling motion.

3. Stability analysis

3.1. Stability with only transversal damping active

Equations of motion (4) gave one of the main advantages in using a non-synchronous damper: it is possible to tune the damping effect by acting not only on the amount of damping (coefficient) but much more on the angular velocity ω_c. A rotor can be stabilized sometimes also without changing the damping coefficients of the dampers. A tuning criterium should be provided to allow engineers to apply it in practice.

Consider the system spinning in the supercritical regime with respect to the first critical speed: instability occurs if the angular velocity exceeds a threshold that, for a Jeffcott rotor, is [3]

$$\sqrt{k/m}\left(1 + c_n/c_r\right). \tag{10}$$

If a non-synchronous damper is added stability can be again assured by varying the angular velocity ω_c: Eq. (4) shows that matrices $\mathbf{C}_r$ and $\mathbf{C}_c$ have equal sign and so it is possible to compensate for the unstable effect of the term $\mathrm{i}\,\omega\,\mathbf{C}_r$ by means of the term $\mathrm{i}\,\omega_c\,\mathbf{C}_c$. Stability analysis is aimed at determining the threshold as a function of the two angular spin speeds ω and ω_c.

To point out the circulatory contribution to the equations of motion let us rewrite them by using real coordinates as follows [3]:

$$\begin{bmatrix} \mathbf{M} & \mathbf{0} \\ \mathbf{0} & \mathbf{M} \end{bmatrix} \ddot{\mathbf{q}}^* + \left(\begin{bmatrix} \mathbf{C} & \mathbf{0} \\ \mathbf{0} & \mathbf{C} \end{bmatrix} + \omega \begin{bmatrix} \mathbf{0} & \mathbf{G} \\ -\mathbf{G} & \mathbf{0} \end{bmatrix} \right) \dot{\mathbf{q}}^* + \left(\begin{bmatrix} \mathbf{K} & \mathbf{0} \\ \mathbf{0} & \mathbf{K} \end{bmatrix} + \omega \begin{bmatrix} \mathbf{0} & \mathbf{C}_r \\ -\mathbf{C}_r & \mathbf{0} \end{bmatrix} + \omega_c \begin{bmatrix} \mathbf{0} & \mathbf{C}_c \\ -\mathbf{C}_c & \mathbf{0} \end{bmatrix} \right) \mathbf{q}^* = \mathbf{f}^*; \tag{11}$$

where $\mathbf{q}^*$ is the vector of the four generalized displacements in real coordinates

$$\mathbf{q}^* = \left\{ x \quad \phi_y \quad y \quad -\phi_x \right\}^{\mathrm{T}} \tag{12}$$

and $\mathbf{f}^*$ is the force vector expressed in terms of real coordinates. The part related to vector $\mathbf{q}^*$ includes a symmetric matrix, which contains the stiffness $\mathbf{K}$, and two skew-symmetric matrices, associated to rotating $\mathbf{C}_r$ and counter-rotating damping $\mathbf{C}_c$. This structure is typical of a circulatory system.

If the condition

$$c_r\,\omega + c_c\,\omega_c = 0 \tag{13}$$

is applied to Eq. (11), it results that the effects of $\mathbf{C}_r$ and $\mathbf{C}_c$ compensate each other. This is due to the assumption that translational co-ordinates are damped, while c_{ϕ_r} is assumed to be null. The skew-symmetric matrices in Eq. (11) related to $\mathbf{q}^*$ vanished and the system is no more circulatory. Thanks to this simplification a first study on the stability of the system can be performed. Kevin, Taft and Chetaev [17] stated in their so-called KTC theorem that for a damped gyroscopic system:

$$\mathbf{M}\,\ddot{\mathbf{q}} + (\mathbf{C} + \mathbf{G})\,\dot{\mathbf{q}} + \mathbf{K}\,\mathbf{q} = \mathbf{0} \tag{14}$$

with $\mathbf{M}=\mathbf{M}^{\mathrm{T}}>0$, $\mathbf{C}=\mathbf{C}^{\mathrm{T}}$, $\mathbf{G}=-\mathbf{G}^{\mathrm{T}}$ and $\mathbf{K}=\mathbf{K}^{\mathrm{T}}$; asymptotical stability [4] is assured when matrices $\mathbf{K}$ and $\mathbf{C}$ are both positive definite. System (11), simplified by condition (13), now has form (14) and the theorem can be applied. Consequently if the angular velocity and the damping coefficients verify relation (13), system (11) is asymptotically stable.

More in general to define a stability map for gyroscopic rotating systems the homogeneous equation associated Eq. (4) can be used. Assuming a solution of the form $z=z_0\,\mathrm{e}^{\mathrm{i}\,\lambda\,t}$, where z_0 is the complex amplitude of the dynamic free response and λ the frequency of the whirling motion, the characteristic equation can be obtained by imposing

$$\det\left[-\mathbf{M}\,\lambda^2+\omega\,\mathbf{G}\,\lambda+\mathrm{i}\,\mathbf{C}\,\lambda+(\mathbf{K}-\mathrm{i}\omega\mathbf{C}_r-\mathrm{i}\omega_c\mathbf{C}_c)\right]=0 \tag{15}$$

or by splitting into the real and imaginary parts:

$$\begin{cases}\mathrm{Re}\left(\left|-\mathbf{M}\,\lambda^2+\omega\,\mathbf{G}\,\lambda+\mathrm{i}\,\mathbf{C}\,\lambda+(\mathbf{K}-\mathrm{i}\omega\mathbf{C}_r-\mathrm{i}\omega_c\mathbf{C}_c)\right|\right)=0,\\ \mathrm{Im}\left(\left|-\mathbf{M}\,\lambda^2+\omega\,\mathbf{G}\,\lambda+\mathrm{i}\,\mathbf{C}\,\lambda+(\mathbf{K}-\mathrm{i}\omega\mathbf{C}_r-\mathrm{i}\omega_c\mathbf{C}_c)\right|\right)=0.\end{cases} \tag{16}$$

Determining the values of the angular velocities (ω,ω_c) for which the system is stable, i.e., a sort of map of stability, is the goal of the analysis. In this situation at least one of the solutions of the system has the form

$$z=z_0\,\mathrm{e}^{\mathrm{i}\,(\alpha+i\,0)\,t}, \tag{17}$$

where the imaginary part of the eigenvalue, i.e., the decay rate of the dynamic response of the system, is set to zero. The stability limit can be obtained assuming that Eq. (15) the imaginary part of λ is equal to zero and the real part equal to α. This method corresponds to the approach proposed in Ref. [18]. By introducing the elements appearing in the matrices and solution (17) into Eqs. (16), it yields

$$m\,J_t\,\alpha^4-m\,J_p\,\omega\,\alpha^3-\left(J_t\,k_{1,1}+m\,k_{2,2}\right)\alpha^2+J_p\,k_{1,1}\,\omega\,\alpha+k_{1,1}\,k_{2,2}-k_{1,2}^2=0, \tag{18a}$$

$$\left(-J_t\,\alpha^2+J_p\,\omega\,\alpha+k_{2,2}\right)\left(c_z\,\alpha-c_{z_r}\,\omega-c_{z_c}\,\omega_c\right)=0. \tag{18b}$$

The following solutions are obtained from Eq. (18b):

$$\alpha_{1,2}=\frac{J_p\,\omega\pm\sqrt{4\,J_t\,k_{2,2}+\omega^2\,J_p^2}}{2\,J_t} \tag{19a}$$

$$\alpha_3=\frac{c_{z_r}\,\omega+c_{z_c}\,\omega_c}{c_z}. \tag{19b}$$

Substituting the first two solutions (19a) into Eq. (18a) all the terms drop out each other and the identity $0=0$ is obtained. Therefore solutions (19a) are not useful to find the analytical expression of the stability thresholds. By introducing solution (19b) in Eq. (18a), it can be found that

$$\begin{aligned}&m\,J_t\left(\frac{c_{z_r}\,\omega+c_{z_c}\,\omega_c}{c_z}\right)^4-m\,J_p\,\omega\left(\frac{c_{z_r}\,\omega+c_{z_c}\,\omega_c}{c_z}\right)^3\\&-\left(J_t\,k_{1,1}+m\,k_{2,2}\right)\left(\frac{c_{z_r}\,\omega+c_{z_c}\,\omega_c}{c_z}\right)^2+J_p\,k_{1,1}\,\omega\left(\frac{c_{z_r}\,\omega+c_{z_c}\,\omega_c}{c_z}\right)\\&+k_{1,1}\,k_{2,2}-k_{1,2}^2=0.\end{aligned} \tag{20}$$

The latter allows to compute the stability thresholds of the system. Eq. (20) can be written in non-dimensional form

$$\left(c'_{z_r}\,\omega' + \omega''_c\right)^4 - J'_p\,\omega'\left(c'_{z_r}\,\omega' + \omega''_c\right)^3 - \left(k'_{2,2}+1\right)\left(c'_{z_r}\,\omega' + \omega''_c\right)^2 + J'_p\,\omega'\left(c'_{z_r}\,\omega' + \omega''_c\right) + k'_{2,2} - k'^2_{1,2} = 0, \tag{21}$$

where

$$\omega' = \frac{\omega}{\sqrt{k_{1,1}/m}}, \quad \omega'_c = \frac{\omega_c}{\sqrt{k_{1,1}/m}}, \quad \omega''_c = \omega'_c\frac{c_{z_c}}{c_z}, \quad J'_p = \frac{J_p}{J_t},$$

$$c'_{z_r} = \frac{c_{z_r}}{c_z}, \quad k'_{2,2} = \frac{k_{2,2}}{J_t k_{1,1}/m}, \quad k'_{1,2} = \sqrt{\frac{k^2_{1,2}}{m\,J_t\left(k_{1,1}/m\right)^2}}.$$

Eq. (21) is used to plot a stability map of the system in terms of non-dimensional angular velocities ω' and ω''_c. On the map it is possible to find, for each value of the angular velocity ω, the values of the angular velocity ω_c of the non-synchronous damper for which the rotor is stable.

Fig. 4 shows the stability maps obtained from Eq. (21) with $c'_{z_r} = 0.1$. A region of stability clearly appears in the middle. In the case of the Jeffcott's rotor the two curves delimiting the stability region in Fig. 4 are simply two straight lines, as shown in Ref. [12]. The gyroscopic terms induce a sort of shift of the stability zone with increasing angular velocity. The two curves have the following asymptotes, for positive values of the non-dimensional angular velocity ω':

$$c'_{z_r}\,\omega' - \omega''_c = 0,$$
$$c'_{z_r}\,\omega' - \omega''_c = 1.$$

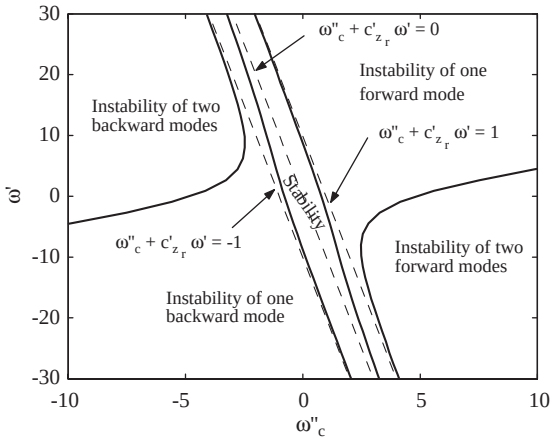

Fig. 4. Stability analysis for the 4 dof system is perfomed in plane ω' (non-dimensional rotor spin speed) versus ω''_c (non-dimensional counter-rotating spin speed). Stability regions are drawn in the presence of damping only applied on the translational motion ($c'_{z_r} = 0.1$).

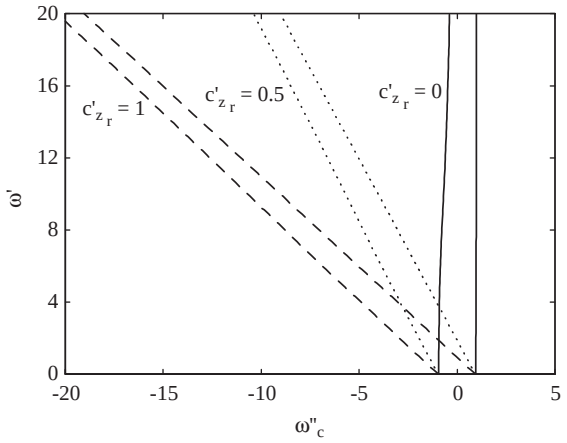

Fig. 5. Stability regions are compared for some values of the non-dimensional damping c'_{z_r} (translational damping coefficient) in plane ω' (non-dimensional rotor spin speed) versus ω''_c (non-dimensional counter-rotating spin speed).

Expression (13) obtained according to the KTC theorem [17] corresponds to one asymptote of the stability curve (Fig. 4) and the asymptote is always inside the stability region. In a machine equipped with a non-synchronous damper, expression (13) can be used as a law to establish, for each value of the rotating speed ω, the angular velocity ω_c of the non-synchronous damper suitable to achieve the stability. For higher values of the rotational speed ω condition (13), shown in Fig. 4 by a straight line inside the stability region, is close to the stability limit. In this situation if any disturbance changes the configuration of the system, the machine could overcome the stability limit and become unstable. Therefore a designer is suggested, for higher angular velocity ω, to operate the rotor slightly far from the neighbourhood described by relation (13).

On the right of the stability zone, forward modes are unstable. In particular, in the first zone the first forward mode is unstable, while in the second one both forward modes are unstable. On the left of the stability zone, a similar situation occurs for the backward modes, both or only one being unstable.

The dependence of the size of the stability zone on the value of non-dimensional rotating damping c'_r is shown in Fig. 5. This parameter spans from 0, for which there is no rotating damping, to 1, in which case there is only rotating damping and other dampings are ineffective. The increasing value of c'_r causes a "rotation" of the stability zone and it is necessary, if the other parameters are left unchanged, to increase the non-dimensional angular velocity ω''_c to obtain the stability of the rotor.

3.2. Stability with damping on both translational and angular co-ordinates

Consider the system modelled by Eq. (4) including a non-vanishing damping coefficient c_ϕ. The stability curves can be drawn again as functions of the angular velocities ω and ω_c,

as already done before. In this case the equations corresponding to Eqs. (18a) and (18b) are

$$m J_t \alpha^4 - J_p m \omega \alpha^3 - \left(c_z c_\phi + J_t k_{11} + m k_{22}\right) \alpha^2 + \left(c_{\phi_r} c_z \omega + c_{z_r} c_\phi \omega + J_p k_{11} \omega + c_\phi c_{z_c} \omega_c\right) \alpha - k_{12}^2 + k_{11} k_{22} - c_{z_r} c_{\phi_r} \omega^2 - c_{\phi_r} c_{z_c} \omega_c \omega = 0, \tag{22a}$$

$$- \left(c_z J_t + c_\phi m\right) \alpha^3 + \left(c_z J_p \omega + c_{z_r} J_t \omega + c_{\phi_r} m \omega + J_t c_{z_c} \omega_c\right) \alpha^2 + \left(c_\phi k_{11} + c_z k_{22} - c_{z_r} J_p \omega^2 - J_p \omega c_{z_c} \omega_c\right) \alpha - c_{\phi_r} k_{11} \omega - c_{z_r} k_{22} \omega - k_{12} c_{z_c} \omega_c = 0. \tag{22b}$$

Now it is impossible to obtain the stability limits from one of the equations after solving the other one in α. An alternative way to plot the stability region is obtaining ω_c from Eq. (22b)

$$\omega_c = \left(-\left(c_z J_t + c_\phi m\right) \alpha^3 + \left(c_z J_p \omega + c_{z_r} J_t \omega + c_{\phi_r} m \omega\right) \alpha^2 + \left(c_\phi k_{11} + c_z k_{22} - c_{z_r} J_p \omega^2\right) \alpha - c_{\phi_r} k_{11} \omega - c_{z_r} k_{22} \omega\right) / \left(c_{z_c} \left(k_{22} + J_p \omega \alpha - J_t \alpha^2\right)\right) \tag{23}$$

and substituting it into Eq. (22a)

$$\begin{aligned} & m J_t^2 \alpha^6 - 2 J_p J_t m \omega \alpha^5 - \left(k_{11} J_t^2 - c_\phi^2 m + 2 J_t k_{22} m - J_p^2 m \omega^2\right) \alpha^4 \\ & - \left(-2 J_p J_t k_{11} \omega + 2 c_{\phi_r} c_\phi m \omega - 2 J_p k_{22} m \omega\right) \alpha^3 \\ & - \left(c_\phi^2 k_{11} + J_t k_{12}^2 - 2 J_t k_{11} k_{22} - m k_{22}^2 + J_p^2 k_{11} \omega^2 - c_{\phi_r}^2 m \omega^2\right) \alpha^2 \\ & - \left(-2 c_\phi c_{\phi_r} k_{11} \omega - J_p k_{12}^2 \omega + 2 J_p k_{11} k_{22} \omega\right) \alpha + k_{12}^2 k_{22} \\ & - k_{11} k_{22}^2 - c_{\phi_r}^2 k_{11} \omega^2 = 0. \end{aligned} \tag{24}$$

The stability curves are computed by assuming a constant value of ω, by solving Eq. (24) as a function of α and introducing the results in Eq. (23). Several values of ω_c related to the value of ω previously assumed are obtained this way.

Stability graphs obtained including the contribution of the damping on the rotational coordinates are quite different from those obtained in the presence of damping only in the translational coordinates. Some numerical examples are shown in Fig. 6. Coefficient c_{ϕ_n} has been set equal to 0.1, 0.01, 0.001 and 0.0001, while c_{ϕ_r} is 0.2 of c_{ϕ_n}. The numerical values for all the other parameters are equal to those used in Fig. 4. Non-dimensional parameters have been introduced to compare the results in the four stability maps of Fig. 6. These stability zones change considerably for different values of damping on the rotational degrees of freedom. The path is irregular and sometimes curves almost cross each other. For higher values of c_{ϕ_n} (0.1) the stability zone splits, while for lower values of c_{ϕ_n} (0.0001) plots similar to Fig. 4 are obtained.

4. Experimental results

4.1. Orbits monitoring

The whirling motion monitoring can be done on the demonstrator by the optical sensors installed. The lateral displacements of the disc detected by the optical sensors were numerically filtered to reduce the noise. Particularly interesting is the evidence of either the occurring

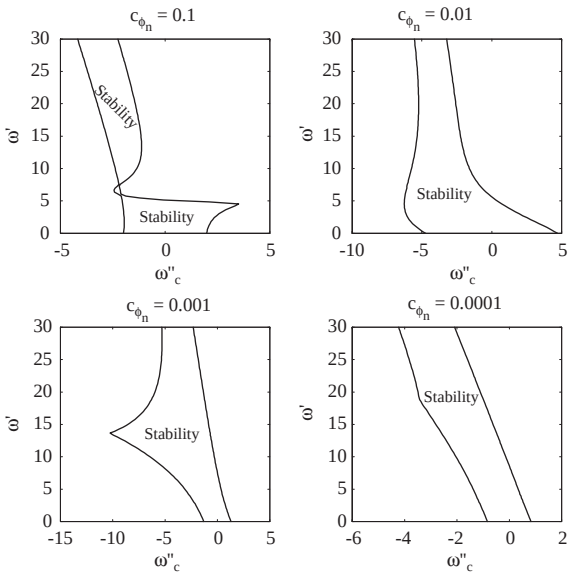

Fig. 6. Stability maps of the system, with both translational and rotational co-ordinates damped, in plane ω' (non-dimensional rotor spin speed) versus ω_c'' (non-dimensional counter-rotating spin speed). Regions are sketched for different values of the damping coefficient c_{ϕ_n} (being fixed $c_{\phi_r} = c_{\phi_n} = 0.2$).

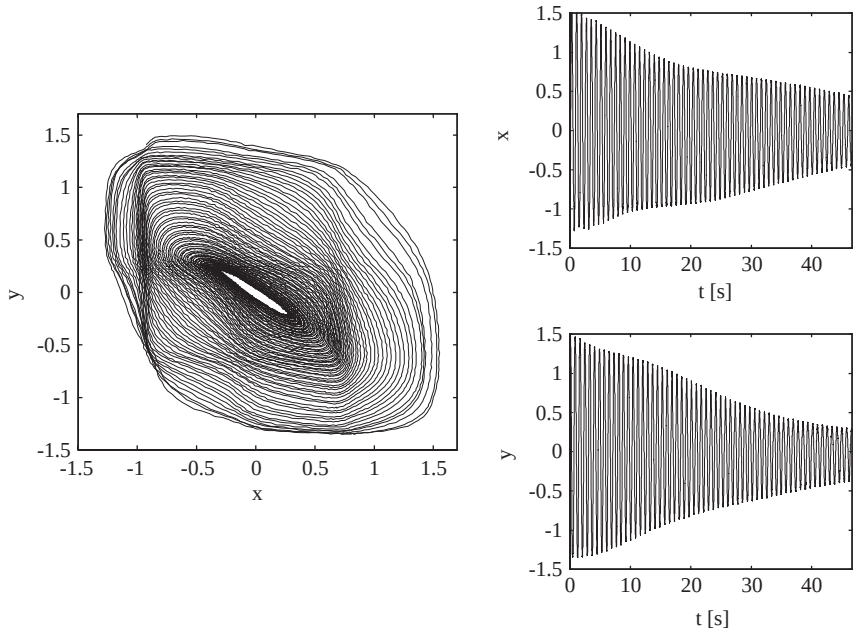

Fig. 7. Orbit and position signals of the first forward whirling mode at standstill.

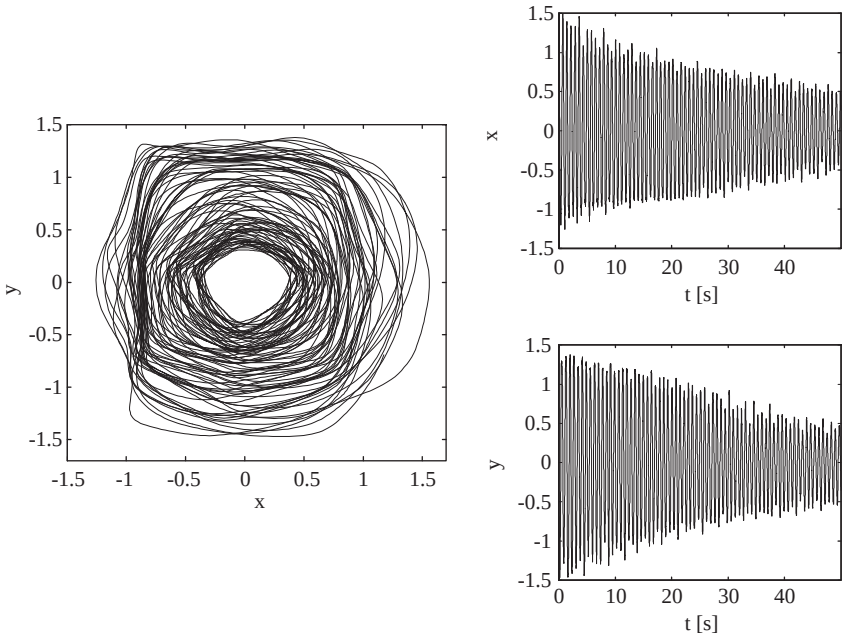

Fig. 8. Orbit and position signals of the first forward whirling mode at 1500 rev/min, and damper standstill.

stabilization or dynamic instability on forward and backward whirls. The standstill dynamic behaviour can be observed by exciting the first forward mode of the pendulum rotor. As Fig. 7 shows, thanks to the non-rotating damping applied by the electromagnetic damper, in this case fixed, the first forward mode appears stable in time, the decay rate of the position signals is positive and their amplitude decreases. If the disc rotates and the damper is still fixed, the orbit documented in Fig. 8 appears stable, at least up to 1500 rev/min, showing a positive decay rate on position signals. In case of counter-rotation of the damper disc if is possible to observe that if one excites the forward mode it is stabilized quite fast by the counter-rotating damping, but after that the first backward mode is excited by the damper and the amplitude of the orbit (Fig. 9) grows exponentially towards the instability. It is remarkable that a slight counter-rotation is favourable to stabilize the forward whirl, but definitely dangerous for the backward whirling, which appears unstabilized.

4.2. Model validation and stability analysis

The above model has been applied to the demonstrator to validate the preliminary statements which came out from the numerical investigations performed and to find the corresponding explanations for the dynamic behaviour documented in the orbit monitoring activity. To predict the dynamic behaviour of the system two models have been built: the 4 dof real one and a FEM model. The resulting Campbell diagram is shown in Fig. 10: the frequencies obtained by the 4 dof model (continuous line), by the FEM model (dashed line) and the experimental results (crosses) are compared. The FEM model was built using DYNROT FEM code for rotordynamic

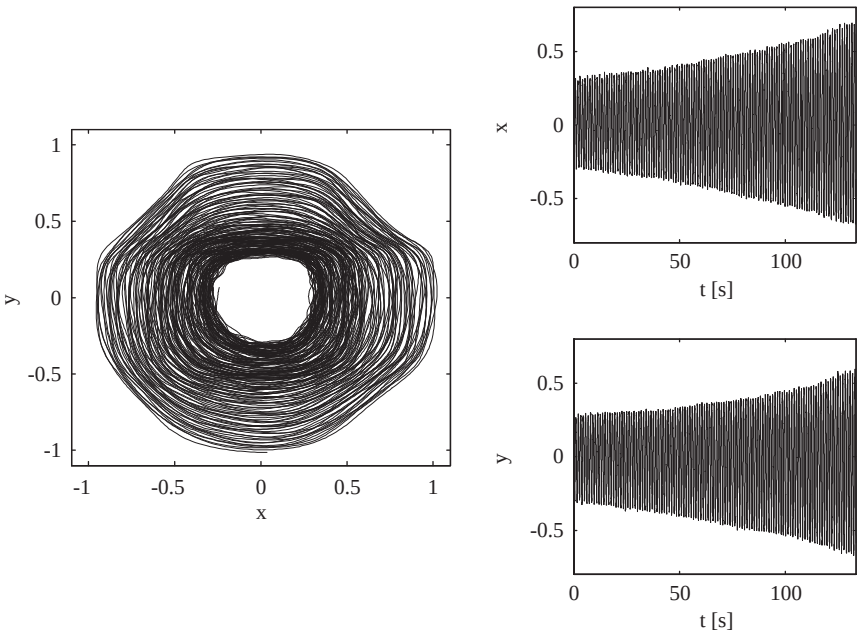

Fig. 9. Orbit and position signals of the first backward whirling mode at 1140 rev/min and damper counter-rotating at 230 rev/min.

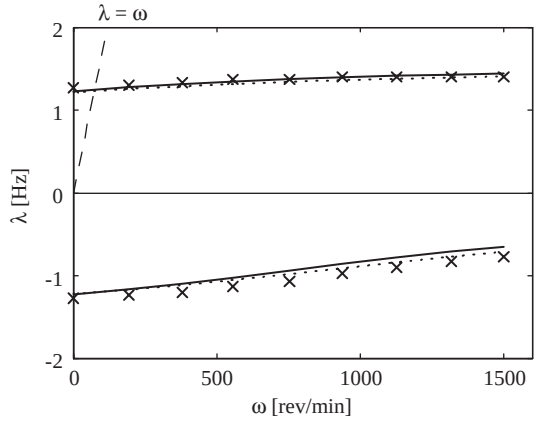

Fig. 10. Campbell diagram of the experimental system: comparison includes analytical model (—), numerical results of the FEM model (Dynrot code) (···) and experimental results (×).

analysis. Only the first forward and backward modes are shown because only these modes are of interest in the demonstration dealing with the stability analysis. The frequency of the position signals monitored by the optical sensors was provided by evaluating the power spectral density through the Welch method of spectral estimation [19]. As Fig. 10 shows, the frequencies obtained from the numerical analysis are close to the experimental ones; nevertheless, the FEM model

approximates experimental results better then the 4 dof model, since it takes into account more accurately for the connection between the disc and the shaft.

To obtain an experimental stability map of the system, the rotating magnetic disc attached to the quill shaft was moved from the equilibrium position and the first mode forward or backward was excited, while the aluminium disc rotated at a constant angular velocity. The amplitude of the oscillations detected by the two optical sensors along two orthogonal directions was recorded by the signal analyzer, and then the orbits were observed. The angular velocity of the aluminium disc was gradually modified until the stability limit was reached, i.e., a constant amplitude of the oscillation was obtained. The stability limits obtained from the experiments (crosses) and using the 4 dof model by neglecting the effect of the damping on the angular co-ordinates are shown in Fig. 11 left . The parameters used in the numerical model are reported in Table 1. The magnetic damping coefficient was approximatively computed in a previous work [20] using an FEM model of the magnetic field and Nagaya's formulas [14]. The damping coefficient of the system was obtained using the structural damping of the quill shaft. Actually most of the system damping is due to the shaft because this element is quite deformable and it dissipates most of the energy. Experimental and numerical curves are in good accordance. In particular, the slope of the curve on the left is quite similar to numerical results even if there is a sort of translation. On the other hand, the curve on the right shows a different slope if compared to numerical values. A tuning on the damping parameters of the model was done in order to obtain a better identify at least under stationaryconditions; damping on the angular co-ordinates was added. New damping coefficients are reported in Table 2. The experimental and theoretical stability limits obtained by using the updated model are reported in Fig. 11-right. The agreement between experimental and numerical values for the forward and backward modes improves by also taking into account the damping related to rotations.

As Fig. 11 shows the whirling conditions monitored and documented in the above paragraph correspond to three working points on the map: the first experiment cited in Fig. 7 is performed in the region of absolute stability, where both backward and forward modes are stable. The second one was performed in the same region by increasing the value of the spin speed from zero up to

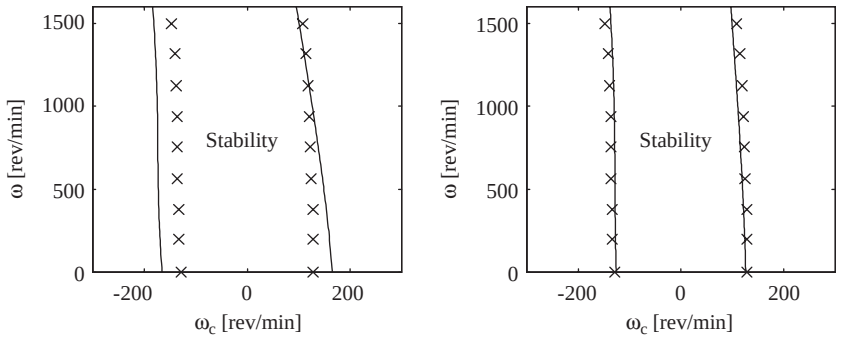

Fig. 11. Stability map of the experimental demonstrator in plane ω (rotor spin speed) versus ω_c (counter-rotating spin speed): comparison between numerical (–) and experimental results (×).

Table 1
Properties of the test rig (nominal values)

Component	Property	Symbol	Value
Magnetic disc	Mass	m	222 g
	Transverse moment of inertia	J_t	7.02×10^{-5} kg/m^2
	Polar moment of inertia	J_p	1.28×10^{-4} kg/m^2
Wire (shaft)	Diameter	d	0.5×10^{-3} m
	Length	l	0.147 m
	Modulus of elasticity	E	2.05×10^{11} N/m^2
Damping coefficients	Non-rotating	c_{z_n}	9.5×10^{-3} N s/m
	Rotating	c_{z_r}	5×10^{-4} N s/m
	Magnetic	c_{z_c}	8×10^{-3} N s/m

Table 2
Tuned damping coefficients used in the upgraded model of the test rig

Translational co-ordinates	Non-rotating	c_{z_n}	9.5×10^{-3} N s/m
	Rotating	c_{z_r}	4.5×10^{-4} N s/m
	Magnetic	c_{z_c}	1.5×10^{-2} N s/m
Angular co-ordinates	Non-rotating	c_{ϕ_n}	10^{-5} N m s/rad
	Rotating	c_{ϕ_r}	8×10^{-7} N m s/rad

1500 r.p.m. In the last case the combination of a rotation at 1140 r.p.m. of the disc and a counter-rotation at 230 r.p.m. of the damper moved the working point on the map towards the instability region of the backward whirling.

5. Conclusions

The main contribution of the present study deals with the mutual interaction between gyroscopic effect and non-synchronous damping in rotating systems. The concept of counter-rotating and co-rotating damping was already investigated in Ref. [12], by neglecting the gyroscopic effect and resorting to the classical Jeffcott rotor. This step was required in order to outline the main role of the non-synchronous rotation on rotor dynamics, when it is associated with any form of dissipation. Industrial applications show that gyroscopic effects are often a relevant aspect of the behaviour of the rotating machinery. An extension of the analytical model proposed in Ref. [12] is used to describe the behaviour of a gyroscopic non-synchronously damped rotor. The analysis is mainly focused on the dynamic stability of a test rig built and modelled with the aim of experimentally verifying the numerical prediction obtained from the

model. The response of a system, where non-synchronous rotating damping affects only translational lateral motions, was first studied. This condition seems to be the most effective in electromechanical coupled eddy current dampers. A relevant result shown by the numerical and experimental investigation is that the stability map of the system includes a region of asymptotic stability for forward and backward whirling achievable by acting on both non-synchronous rotation and damping coefficient also when gyroscopic effects are accounted for. The stability zone depends on both rotor and non-synchronous angular speeds. Instability can affect one or two modes; furthermore, backward modes can be unstabilized if counter-rotation is too fast. An interesting effect is that the value of the rotating damping coefficient causes a rotation of the stability region about the thresholds at zero spin speed of the rotor. When the non-synchronous rotating damping coefficient related to the rotational degree of freedom of the rotor is taken into account, the neighbourlines of the regions of the map of stability become irregular, if compared to the previous case, depending on the numerical value of the coefficient itself, and for lower values it appears similar to those previously computed. Experiments performed using an eddy current damper acting on a disc suspended by a quill shaft confirm that the model is able to predict the behaviour of non-synchronously damped systems in terms of natural frequency and stability thresholds. In particular, both the contributions affecting the translational and rotational co-ordinates are important to predict correctly the region of stability of a gyroscopic rotor.

References

[1] F.M. Dimentberg, *Flexural Vibrations of Rotating Shafts*, Butterworths, London, 1961.
[2] M. Lalanne, G. Ferraris, *Rotordynamics Predictions in Engineering*, New York, Wiley, 1990.
[3] G. Genta, *Vibration of Structures and Machines*, 3rd Edition, Springer, New York, 1998.
[4] P.C. Hughes, *Spacecraft Attitude Dynamics*, Wiley, New York, 1986.
[5] A.M. Nobili, D. Bramanti, E. Polacco, G. Catastini, A. Milani, L. Anselmo, M. Andrenucci, S. Marcuccio, A. Genovese, F. Scortecci, G. Genta, C. Delprete, E. Brusa, D. Bassani, G. Vannaroni, M. Dobrowolny, E. Melchioni, C. Arduini, U. Ponzi, G. Laneve, D. Mortari, M. Parisse, F. Curti, F. Cabiati, E. Rossi, A. Sosso, G. Zago, S. Monaco, G. Gori Giorgi, S. Battilotti, L. Dantonio, G. Amicucci, Galileo Galilei flight experiment on equivalence principle with field emission electric propulsion, *Journal of the Astronautical Sciences* 43 (3) (1995) 219–242.
[6] A.M. Nobili, D. Bramanti, G. Catastini, E. Polacco, G. Genta, E. Brusa, V.P. Mitrofanov, A. Bernard, P. Touboul, A.J. Cook, J. Hough, I.W. Roxburgh, A. Polnarev, W. Flury, F. Barlier, C. Marchal, Proposed noncryogenic, nondrag-free test of the eqivalence pinciple in space, *New Astronomy* 3 (1998) 175–218.
[7] G. Genta, C. Delprete, E. Brusa, Some considerations on the basic assumptions in rotordynamics, *Journal of Sound and Vibration* 227 (3) (1999) 611–645.
[8] G. Genta, E. Brusa, Fast-spinning multibody spacecrafts seen as free rotors: stability considerations, *Space Forum* 2 (1999) 319–344.
[9] S.H. Crandall, *Engineering Analysis: A Survey of Numerical Procedures*, McGraw-Hill, New York, 1956.
[10] S.H. Crandall, A heuristic explanation of journal bearing instability, in: *Rotordynamics Instability Problems in Turbomachinery*, NASA CP-2250, 1982.
[11] J.W. Lund, Stability and damped critical speeds of a flexible rotor in fluid-film bearings, in: *Rotating Machinery Dynamics*, Vol. 1, ASME, 1987.
[12] G. Genta, E. Brusa, On the role of non-synchronous rotating damping in rotordynamics, *International Journal of Rotating Machinery* 6 (6) (2000).
[13] G. Genta, E. Brusa, Active stabilization of a fast-spinning multibody spacecraft, 48*th IAF International Astronautical Congress*, 1997.

[14] K. Nagaya, H. Kojima, On a magnetic damper consisting of a circular magnetic flux and a conductor of arbitrary shape. Part I: derivation of the damping coefficients, *Journal of Dynamic Systems, Measurement, and Control* 106 (1984) 46–51.
[15] K. Nagaya, On a magnetic damper consisting of a circular magnetic flux and a conductor of arbitrary shape. Part II: applications and numerical results, *Journal of Dynamic Systems, Measurement, and Control* 106 (1984) 52–55.
[16] G. Genta, C. Delprete, A. Tonoli, E. Rava, L. Mazzocchetti, Analytical and experimental investigation of a magnetic radial passive damper, *Proceedings of the Third International Symposium on Magnetic Bearings*, July 29–31, Alexandria, 1992, pp. 255–264.
[17] E.E. Zajac, The Kelvin–Taft–Chetaev theorem and extensions, *Journal of the Astronautical Sciences* 11 (2) (1964) 46–49.
[18] Z.A. Parszewski, J.M. Krodkiewski, J. Skoraczynski, Stability assessment of machine systems described by receptance, *Journal of Sound and Vibration* 120 (3) (1988) 527–538.
[19] S.L. Marple, *Digital Spectral Analysis with Applications*, Prentice-Hall, Englewood Cliffs, NJ, 1987.
[20] M. Cavallero, Construction and Tests on a Didactic Demonstrator for the Dynamic Behaviour of Rotors without Statoric Supports, Master Thesis, Politecnico di Torino, 1997.